ELSEVIER

Journal of Photochemistry and Photobiology A: Chemistry 142 (2001) 107–119

Journal of Photochemistry and Photobiology A:Chemistry

www.elsevier.com/locate/jphotochem

The mechanism of energy transfer in the antenna of photosynthetic purple bacteria

Mino Yang*, Ritesh Agarwal, Graham R. Fleming

Department of Chemistry, Lawrence Berkeley National Laboratory, Physical Biosciences Division, University of California, Berkeley, CA 94720, USA

This paper is dedicated to Lord Porter on the occasion of his 80th birthday.

Abstract

The mechanism of energy transfer in the antenna system of purple bacteria is investigated by combination of photon echo spectroscopy and disordered exciton theory. In the B800 component of light harvesting complex 2 (LH2), a picture of incoherent hopping between monomers provides an excellent description of the photon echo data recorded as a function of excitation wavelength. In the B850 pigments of LH2, and to a somewhat greater extent in the B875 pigments of light harvesting complex 1 (LH1), the excitation is delocalized over several pigments. The observed dynamics correspond to relaxation between exciton states as a result of exciton–phonon coupling. Nonetheless, a picture of "hopping" between small groups of molecules provides a crude description of the motion of the excitation in B850, and B875. The electronic coupling required to simulate the experimental absorption spectrum and photon echo data is larger in LH1 than in LH2 (B850). © 2001 Published by Elsevier Science B.V.

Keywords: Purple bacteria; Antenna; Photosynthesis

1. Introduction

The process of light harvesting in which several hundred chlorophyll or bacteriochlorophyll molecules act as an antenna to collect and direct solar energy to a reaction center is central to the efficiency of terrestrial photosynthesis. Often, the overall efficiency of energy transfer from the antenna to the reaction center is above 95%, an astonishing fact given that the excitation must be transferred hundreds of times, and that the energy transfer efficiency of a spatially random solution of chlorophyll at the concentration (i.e. number density) of the chloroplast is vanishingly small.

The work of Lord Porter over the past half century has stimulated and inspired much of modern research on photosynthetic light harvesting. During this period, methods of temporal and spatial resolution have steadily improved along with the theoretical tools necessary to interpret and even predict the dynamical behavior of photosynthetic systems. Porter et al. [1] (and independently Alfano et al. [2,3] and Shapiro et al. [4]) were the first to use the picosecond time resolved spectroscopy to study energy migration in the antenna systems of plants and algae. Perhaps the culmination of this pioneering work was the beautiful demonstration of the energy funnel in phycobilisomes with the clear sequential population of progressively lower energy species as the energy flows through the phycobilisome to the core reaction center complex [5]. In parallel with these elegant experiments, Porter's group was pursuing some of the puzzling theoretical issues in light harvesting. Of particular significance was the demonstration by Beddard and Porter [6] of the role of concentration quenching in spatially random arrangements of chlorophyll molecules, and the consequent suggestion that chlorophyll molecules must be held in fixed positions in close (say 12 Å) proximity, but not allowed to come into full electronic contact. This was an extremely important suggestion at the time because it was not universally accepted (especially in the USA) that the antenna chlorophylls were bound exclusively in protein complexes rather than being in the lipid membrane. Of course, subsequent X-ray crystallographic studies have shown that all antenna molecules are bound in pigment–protein complexes in fixed and generally in highly organized arrangements [7–13].

The ability to obtain high resolution structures of membrane proteins, first of the reaction center [14–17] followed by the peripheral light harvesting complex of purple bacteria LH2 [7–9] has revolutionized our understanding of the primary steps of photosynthesis. At the time of writing, high resolution structures of photosystems I and II (PSI and PSII) of cyanobacteria and green plants have been announced and will be published shortly. These structures allow questions of mechanism and structure/function/dynamics relationships to

* Corresponding author.
E-mail address: minoyang@uclink4.berkeley.edu (M. Yang).

1010-6030/01/$ – see front matter © 2001 Published by Elsevier Science B.V.
PII: S1010-6030(01)00504-4

be brought into sharp relief. In parallel with the advances in structure determination, advances in ultrafast spectroscopy and in theoretical chemistry allow many of these fundamental questions to be addressed at a quantitative level.

Two such fundamental questions can be simply stated. (1) What is the interaction mechanism between the chromophores in such densely packed molecular aggregates? Is it the standard point dipole–dipole interaction responsible for long range energy transfer between strongly allowed transitions or do different mechanisms, perhaps arising from orbital overlap contribute or even dominate when donors and acceptors are spaced by distances less than their size? A related question concerns the role of 'dark' states, i.e. states with forbidden transitions in the energy migration process. Can such states play a role and if so, what is the mechanism? (2) Given that electronic couplings between individual molecules may be large compared to their reorganization energies and static variations in their energy levels, what is the mechanism by which excitation energy moves in the antenna? Is it appropriate to describe the process as incoherent hopping between individual molecules, or is the excitation at least partially delocalized over several or many molecules, moving in a coherent fashion? To elaborate the question a little, what states does the excitation process prepare and how do they evolve? Does the excitation become localized over time and if so, what is the timescale compared to energy migration and overall trapping?

Answers to these two questions should help to elucidate the design principles underlying the efficiency of photosynthetic light harvesting and inform the design and synthesis of synthetic antenna devices, such as dendrimeric light harvesting systems ([18] and references therein). In this paper, we describe calculations and experiments designed to answer both questions in the context of the purple bacterial antenna complexes LH2 and LH1. The structure of LH2 is shown in Fig. 1, while the structure of LH1 is believed to be very similar to LH2 but with a larger ring containing 16 dimeric subunits (32 bacteriochlorophyll (BChl) molecules) rather than the 8 [9] or 9 [7] (16 or 18 BChls) dimeric subunits in LH2. In addition, LH1 lacks the ring of nine (in the *Rps. acidophila* structure) apparently monomeric BChl molecules present in LH2. Both structures also contain carotenoid molecules (see Fig. 1) acting in both protective and light harvesting roles [19]. The excited states of carotenoids, in common with other long chain polyenes, are unusual. The first excited singlet-state is of nominal A_g symmetry and thus, optical transitions from the ground state are one-photon forbidden. The transition to the second singlet state is strongly allowed and can couple to the BChl molecules via the standard Coulombic mechanism. However, the location and effectiveness in energy transfer of the first singlet state has been, until very recently, quite unclear. With the notable exceptions, [20–22] it has generally been supposed by most previous workers that the coupling of the S_1 state to the BChl molecules occurs via the Dexter exchange mechanism [23]. As we have shown elsewhere, this is incorrect and the Coulombic coupling mechanism also mediates very rapid ($\sim$1 ps) energy transfer from the carotenoid S_1 state to the BChls, even though no absorption band for these states is detectable in the one-photon spectrum [24,25].

In this paper, we focus on the electronic interactions and energy transfer mechanisms in the three distinct sets of BChl molecules in the antenna system of purple bacteria: B800 and B850 of LH2 and B875 of LH1. Because the

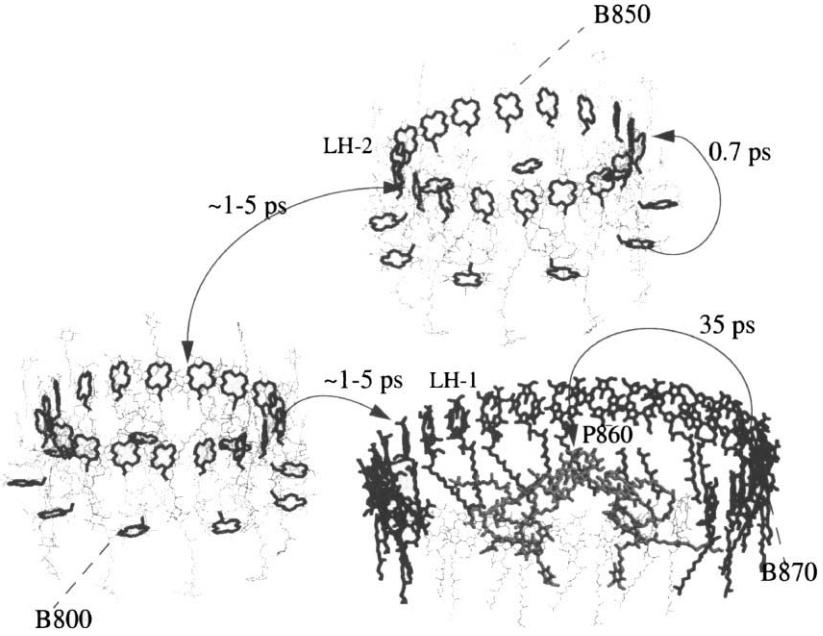

Fig. 1. Schematic view of the light harvesting antenna system of purple bacteria. The structure of LH2 is from [7] while that of LH1 is based on [10,66]. LH1 is shown cut away to show the reaction center.

electronic interactions between the chromophores are relatively weak, energetic disorder, which is an inevitable feature of self-assembled systems, plays a major role in determining the electronic structure and dynamics. Study of such systems is greatly aided by experimental techniques that are sensitive to distributions of optical transition frequencies. Photon echo spectroscopy in general and the three-pulse photon echo peak shift technique in particular give incisive information about dynamics in inhomogeneous systems. In contrast, more traditional approaches, such as spontaneous fluorescence or transient absorption spectroscopy are quite insensitive to the nature of inhomogeneous dynamics. We, thus, focus our paper on photon echo measurements and their analysis via theoretical models.

2. The measurement of photosynthetic energy transfer via photon echo spectroscopy

While the pioneering picosecond measurements of Porter, Treadwell, Beddard, and coworkers gave access to overall energy trapping timescales, the timescale of energy transfer between individual molecules was inaccessible before the development of sub-100 fs laser sources. Although in reality, a continuum of possibilities exist, for the purpose of organizing this discussion we will distinguish two types of energy transfer: intra- and inter-band transfer. By the former, we mean transfer to molecules of similar spectral character whose absorption band lies within the spectrum of the laser used for excitation. An example of this, intraband transfer is the transfer within the B800 or B850 rings of LH2 (see Fig. 1) or the B875 ring of LH1. In interband transfer, the excitation moves to a species absorbing outside the excitation laser spectrum, examples being B800 to B850 transfer, or carotenoid to either B800 or B850 transfer in LH2. Clearly, the interband transfers, given adequate time resolution, are accessible to the standard methods of pump-probe and fluorescence upconversion spectroscopy. However, the intraband cases are just those where electronic delocalization effects might be most important since the energy gaps between molecules are small, allowing the possibility of strong coupling.

Over the past 5 years, we have been developing a type of photon echo measurement, the three pulse echo peak shift method (3PEPS) which seems specially suited to the measurement of intraband energy transfer [26–47]. The 3PEPS technique has been described in detail elsewhere [27,48,49], and here we will confine ourselves to a brief description of the information content of the technique and some recent developments. A peak shift, $\tau^*(T)$, plot, such as the one shown in Fig. 2 is obtained by determining the position of the three pulse echo profile maximum with respect to zero delay for the coherence period (τ) as a function of the population period, T. Fig. 2 shows peak shift data for a dilute solution of a dye molecule IR144 in a polymer glass PMMA [30,36]. The long-time value of the peak shift is finite,

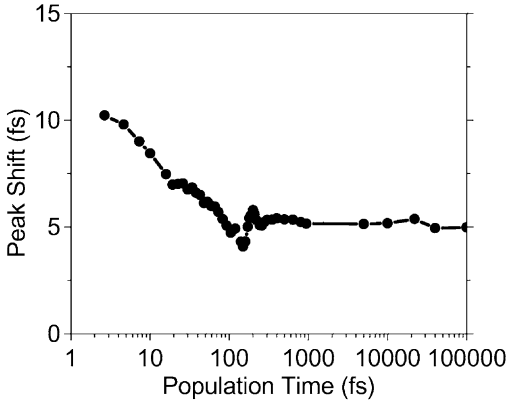

Fig. 2. Plot of the three pulse echo peak shift for a dilute solution of the dye IR144 in PMMA at room temperature [30]. The oscillatory features result from vibrational wavepackets. Note that the peak shift ($\tau^*(T)$) becomes consistent after about 200 fs, whereas in fluid solution, the peak shift decays to zero on a picosecond timescale.

unlike the case of a fluid solution, [48] and reflects the presence of static inhomogeneous broadening in the transition frequencies of the individual chromophores.

Now consider an ensemble of molecular aggregates, each aggregate consisting of a set of chemically identical chromophores. Fig. 3 shows two possible scenarios for the distribution of site energies (and optical transition frequencies) for the chromophores. In the first picture, the mean energy of each aggregate is the same, in other words, the energies of each member of the aggregate are chosen at random from the full distribution and have no correlation with each other. In the second case, there is some correlation between individual members of a particular ensemble and as a consequence, the means of the individual aggregates are also distributed. In this context, we can write the static energy (or transition energy) of an individual chromophore, i, in aggregate 'a' as

$$\varepsilon_{\mathrm{a}}^{i} = \langle\varepsilon\rangle + E_{\mathrm{a}} + \delta\varepsilon_{\mathrm{a}}^{i} \tag{1}$$

where $\langle\varepsilon\rangle$ is the mean energy of the monomers over the whole ensemble, E_{a} the static offset of the mean energy of the monomers in the aggregate a from $\langle\varepsilon\rangle$ and $\delta\varepsilon_{\mathrm{a}}^{i}$ is the static offset of the energy of the chromophore, i, from E_{a}. The standard deviations of the distributions of E_{a} and $\delta\varepsilon_{\mathrm{a}}^{i}$

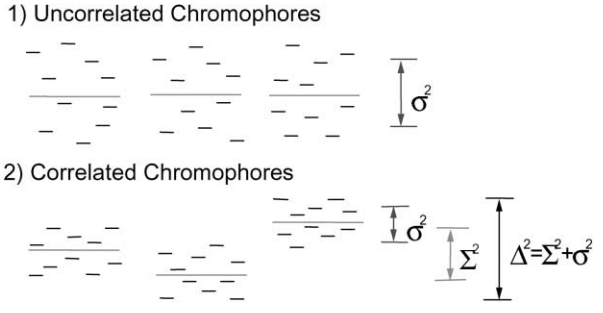

Fig. 3. An illustration of the two types of disorder discussed in the text.

are defined by Σ and σ, respectively, and the total inhomogeneous width is given by

$$\Delta^2 = \Sigma^2 + \sigma^2 \quad (2)$$

The energy transfer time within an aggregate or the size of the delocalization of an exciton state depends only on σ. On the other hand, the energy transfer time scale between aggregates will depend mainly upon Σ. The bandwidth of the absorption spectrum will depend on both quantities. Thus, the characterization of these quantities is important.

In photon echo experiments, the presence of static inhomogeneous broadening allows rephasing because the memory of a given molecule's transition frequency is retained (totally in the absence of homogeneous dephasing, partially in the presence of both inhomogeneous and homogeneous dephasing). In the peak shift measurement, this leads to a finite long-time value of the peak shift, $\tau^*(\infty)$. This discussion applies to a dilute system in which excitation remains confined to the molecule that was initially excited. Now in a molecular aggregate in which energy transfer occurs between individual monomers, the excitation can explore the σ distribution, but the Σ distribution either not at all, or on a much longer timescale. Thus, the energy transfer process itself leads to a loss of transition frequency memory and, thus, a decay of the peak shift. The timescale of the energy transfer is represented directly in the dependence of the τ^* on T. If $\Sigma = 0$, the energy transfer will lead to complete loss of memory and $\tau^* = 0$ at longer time than energy transfer time scale. If $\Sigma \neq 0$, this is not so and the form of $\tau^*(T)$ can be used to determine both Σ and σ [45,50]. Fig. 4 shows the remarkable sensitivity, in the presence of intraband energy transfer, to the site energy distributions of the 3PEPS method. By contrast, both transient absorption and transient grating methods are quite insensitive to the presence or absence of intraband energy transfer in such a system; still less the nature of the ensemble disorder (Fig. 4).

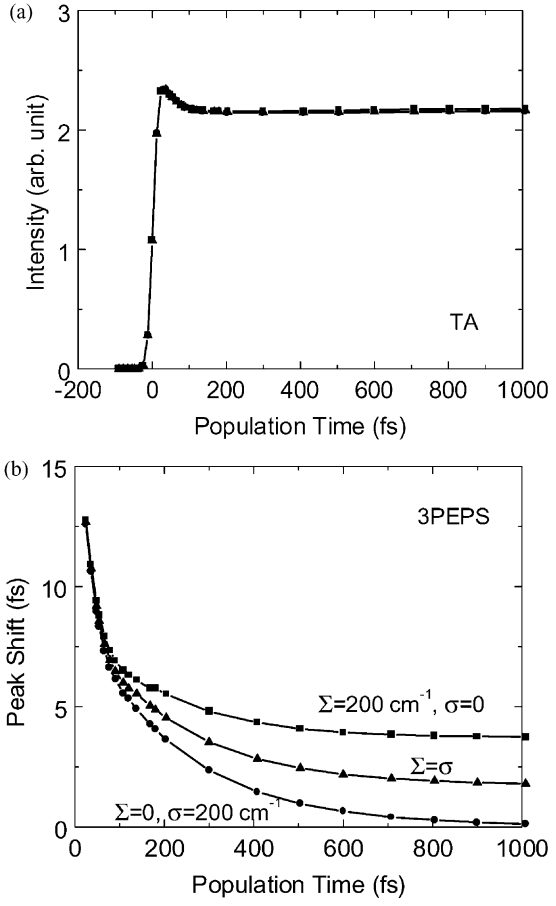

Fig. 4. Calculated transient absorption (TA) (a) and peak shift (3PEPS) (b) signals for three different energy transfer systems with (i) completely uncorrelated disorder ($\Sigma = 0, \sigma = 200\,\mathrm{cm}^{-1}$); (ii) partially correlated $\Sigma = \sigma = 141\,\mathrm{cm}^{-1}$; (iii) completely correlated ($\Sigma = 200\,\mathrm{cm}^{-1}, \sigma = 0$). All three curves are essentially identical for TA, but give very different results in 3PEPS.

Before describing a specific light harvesting system, it is worthwhile exploring the origins of the σ and Σ distributions a little further. The individual sites of particular chromophores can give rise to variations in the transition frequency for a variety of reasons. For example, side chain conformational disorder undoubtedly exists in the polypeptides that bind the chromophores. Ionizable side chains may be close to their pK and thus distributed between charged and neutral forms. The transition frequency of chlorophyll molecules is known to be quite sensitive to distortions of the macrocycle from planarity [51]. Any or all of these effects (originating from local inhomogeneities around a chromophore) will contribute to σ.

There are two types of contribution to Σ: the first has been previously discussed in the context of single molecule spectroscopy [52–54] and arises from global distortions of the whole complex, thus shifting the mean transition frequency of the entire set of chromophores in the complex. Several research groups have introduced this variable based on the physical heterogeneity among the aggregates and the mechanisms producing the fluctuations in E_a and $\delta\varepsilon_a^i$ have often been implicitly assumed to be independent. In this case, the aggregate energy will be different from one aggregate to another and, thus, the introduction of a stochastic variable, E_a, for the aggregate energy is required. For example, Freiberg et al. attribute the fluctuation of E_a to random solvent shifts and the fluctuations of $\delta\varepsilon_a^i$ to different environments surrounding the monomers [52]. van Oijin et al. also introduced intra- and inter-complex heterogeneity but without any specific mechanism [53]. Mostovoy and Knoester successfully analyzed recent single molecule spectra by employing inter-ring disorder [54]. They suggested that the sources of the inter-ring disorder could be structural deformation or finite correlation between monomers with a ring. Agarwal et al. also used a two-level disorder model to explain their 3PEPS data and linear absorption spectrum of B800 in LH2 [50].

The second contribution to Σ is purely statistical and does not seem to have been discussed earlier. This effect arises from the fact that each individual aggregate samples

a rather small portion of the total distribution (originating from the local inhomogeneities around a chromophore). The fact that the number of monomers in a given aggregate is not sufficient to fully sample the distribution, necessarily produces a distribution in the means of the individual complexes. We will refer to this finite sampling contribution to Σ as Σ_{loc} whereas the global distortion contribution we denote as Σ_{glob}.

Assuming these two are independent, we have

$$\Sigma^2 = \Sigma_{\mathrm{glob}}^2 + \Sigma_{\mathrm{loc}}^2 \tag{3}$$

and, equivalently, the total inhomogeneous width

$$\Delta^2 = \Sigma_{\mathrm{glob}}^2 + \Sigma_{\mathrm{loc}}^2 + \sigma^2 \equiv \Sigma_{\mathrm{glob}}^2 + \Delta_{\mathrm{loc}}^2 \tag{4}$$

One can easily realize from simple Gaussian statistics that

$$\Sigma_{\mathrm{loc}} = \frac{\Delta_{\mathrm{loc}}}{\sqrt{N}} \tag{5}$$

which means the aggregate energy fluctuates with Gaussian statistics characterized by Σ_{loc} (unless $N \to \infty$) even in the absence of any global fluctuation of a whole complex. In this case, the standard deviation of the intra-aggregate fluctuation σ is written in terms of the total fluctuation width of the local inhomogeneities, Δ_{loc}, as

$$\sigma = \sqrt{\Delta_{\mathrm{loc}}^2 - \Sigma_{\mathrm{loc}}^2} = \Delta_{\mathrm{loc}}\sqrt{\frac{N-1}{N}} \tag{6}$$

Then if the inter-aggregate disorder originates only from this kind of statistical effect, i.e. $\Sigma = \Sigma_{\mathrm{loc}}$, we arrive at a simple relation between Σ and σ

$$\frac{\sigma}{\Sigma} = \sqrt{N-1} \tag{7}$$

and the effect of inter-aggregate disorder will relatively increase when the number of monomers is small as in the B800 band of LH2.

Fig. 5 illustrates the statistical contribution to Σ. In the upper panel, the open circles show the distribution of transition frequencies of individual monomers randomly chosen from a Gaussian distribution. The solid bars show the means of individual complexes containing nine monomers, and are clearly characterized by a distribution of their own. The lower panel quantifies this relationship showing the standard deviations within a complex (intra, open circles) and between complexes (inter, filled squares) as a function of the number of monomers. As an example, consider the B800 component of LH2 in *Rps. acidophila*, which contains nine monomers per LH2. If the total inhomogeneous width (Δ_{loc}) is $100\,\mathrm{cm}^{-1}$, from Eqs. (5) and (6), we expect $\sigma = 94\,\mathrm{cm}^{-1}$ and $\Sigma_{\mathrm{loc}} = 34\,\mathrm{cm}^{-1}$.

We can compare the predictions of Eq. (7) with some literature data. Freiberg et al. simulated the linear and nonlinear spectra of both the B800 and B850 bands of LH2 [52]. They concluded that $\sigma^{\mathrm{B850}} = 216\,\mathrm{cm}^{-1}$, $\Sigma^{\mathrm{B850}} = 54\,\mathrm{cm}^{-1}$; $\sigma^{\mathrm{B800}} = 46\,\mathrm{cm}^{-1}$, $\Sigma^{\mathrm{B800}} = 46\,\mathrm{cm}^{-1}$ which give ratios

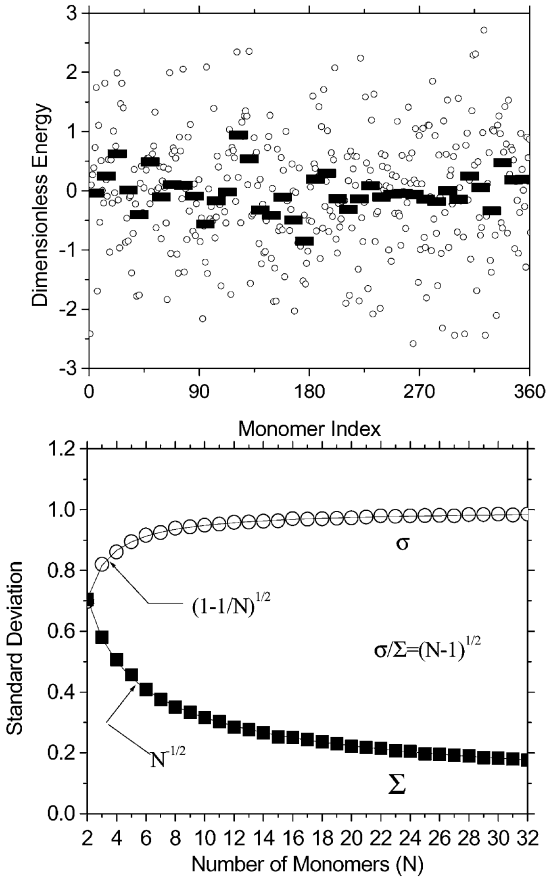

Fig. 5. Upper panel: plot of distribution of monomer energies (open circles) for 360 monomers chosen from a Gaussian distribution of standard deviation, 1. The bars indicate the mean energies of sets of nine chromophores chosen from the distribution. Lower panel: plot of standard deviation within a complex (open circles) and between complexes (filled squares) as a function of the number of monomers in a complex.

of $\sigma^{\mathrm{B850}}/\Sigma^{\mathrm{B850}} = 4$ and $\sigma^{B800}/\Sigma^{B800} = 1$. We can see the ratio for the B850 surprisingly agrees well with Eq. (7) which gives 4.1, but the ratio for the B800 is different from our estimate of 2.8 and from Agarwal et al.'s value of 1.8 (see Section 3.1). However, the qualitative finding that the ratio decreases with decreasing numbers of monomers is in accordance with Eq. (7) and, thus, we conclude that a significant portion of the inter-aggregate disorder they observed arises from statistical fluctuations.

Since $\sigma \approx \Delta_{\mathrm{loc}}$, as can be seen in Eq. (6), for typical LH complexes, the influence of different levels of local inhomogeneity may be difficult to observe in studies concentrating on the electronic structure and dynamics occurring only within one aggregate [55]. However, when the intra-aggregate properties are combined with optical properties affected by overall distribution of energy (in most ensemble-averaged experiments and even in some single molecule spectroscopy studies [52–54]), one should carefully describe this second level of static disorder.

3. Nonlinear response of weakly coupled systems

In order to model an actual photosynthetic complex, a detailed model for the population dynamics is required. Since the rate of energy transfer between chromophores i and j will depend on their energies in disordered systems, it is necessary to properly account for the ensemble effect. Noting the optical responses from energy donors (excited by laser) and acceptors (excited by energy transfer) have different characteristics, Yang and Fleming showed that, for weakly coupled systems, to a reasonable approximation the nonlinear optical signal can be written as [45]

$$\text{Signal} \approx \langle R_{\mathrm{D}}\rangle_{\text{disorder}} \cdot \langle P_{\mathrm{D}}\rangle_{\text{disorder}} + \langle R_{\mathrm{A}}\rangle_{\text{disorder}} \cdot \langle P_{\mathrm{A}}\rangle_{\text{disorder}} \quad (8)$$

where $\langle R_{\mathrm{D(A)}}\rangle_{\text{disorder}}$ and $\langle P_{\mathrm{D(A)}}\rangle_{\text{disorder}}$ are the ensemble-averaged optical response function and population, respectively, of energy donors (acceptors). The factorization in Eq. (8) neglects any correlation between inhomogeneous optical responses and inhomogeneous population kinetics and is a mean kinetics approximation. With this factorization, instead of full Monte Carlo computation in three dimensions (with respect to time variables in the third-order experiments), we can carry out a Monte Carlo procedure only for the population kinetics as described below and then combine those with analytic expressions for the optical response functions [45] to make the simulation much more efficient.

For a given configuration of static energies of chromophores, we calculate the time dependent population using the Pauli master equation

$$\frac{\mathrm{d}}{\mathrm{d}t}P_i(t) = -\tau_i^{-1}P_i(t) - \sum_{\substack{j=1\\ j\neq i}}^{N}[F_{ji}P_i(t) - F_{ij}P_j(t)] \quad (9)$$

Here F_{ij} is the rate constant for transfer from site j to site i, $P_i(t)$ the probability of occupation of site i, τ_i the lifetime of the excited state, which in this care corresponds to the B800 to B850 energy transfer time. Downhill rates are calculated from the overlaps of site-energy-dependent donor emission and acceptor absorption spectra, while uphill rates are calculated via the detailed balance equation

$$F_{ji} = F_{ij}\exp\left(\frac{-\Delta E_{ji}}{k_{\mathrm{B}}T}\right) \quad (10)$$

where ΔE_{ji} is the difference between the peak frequencies of the donor and acceptor absorption bands. The effect of disorder on energy transfer rate appears directly through the overlap integral between two chromophores with their own site energies. The Pauli master equation is solved using the Green function solution of the coupled equations [56]. Each chromophore is assigned a site energy randomly chosen from a Gaussian distribution by a Monte Carlo sampling procedure and then the averaged populations are inserted into Eq. (8). In order to model the data of Fig. 6, we input the homogeneous lineshape, the coupling strength and the laser spectrum. The energy transfer rates are calculated from these parameters within the model.

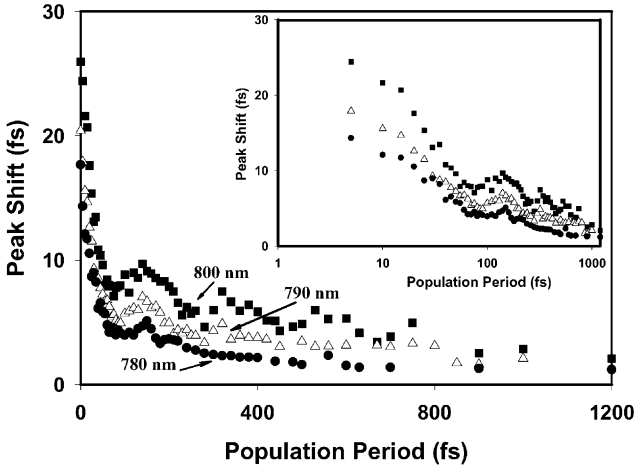

Fig. 6. Peak shift data for the LH2 complex of *Rps. acidophila* at three different wavelengths within the B800 band. Inset shows the same data on a logarithmic timescale.

3.1. Application to the B800 band of LH2

The approach described above has been applied to photon echo data for the B800 band of LH2 [50]. In this work, pulses of 25 fs were used. These pulses have a bandwidth which covers the entire absorption band of the B800 chromophores. The intraband energy transfer was shown to occur with an average timescale of 500–600 fs [50,57,58]. Further, it was not possible to describe the data using only a value for σ. The data were best fit by $\sigma = 90\,\mathrm{cm}^{-1}$ and $\Sigma = 50\,\mathrm{cm}^{-1}$ ($\Delta = 103\,\mathrm{cm}^{-1}$). The values are extremely close to those expected if $\Sigma = \Sigma_{\mathrm{loc}}$, in other words, the variations in the mean energies of the B800 sets in individual LH2 complexes appears to arise almost entirely from the limited sampling effect illustrated in Fig. 5.

The coupling between the B800 molecules in LH2 is calculated to be $30\,\mathrm{cm}^{-1}$, [57,59,60] which is small compared to the homogeneous linewidth, disorder, and thermal energy ($k_{\mathrm{B}}T$). We, therefore, expect a model based on incoherent hopping in an inhomogeneous ensemble to accurately describe the energy transfer dynamics. To test this idea in detail, we carried out excitation wavelength dependent 3PEPS studies with excitation pulses centered at 800, 790, and 780 nm. The results of these experiments are shown in Fig. 6. All three peak shift curves show the presence of $165\,\mathrm{cm}^{-1}$ vibrational wavepackets persisting up to at least 1 ps at 800 nm. The amplitude of the quantum beats decreases with excitation wavelength as does the initial value of the peak shift. Both of these effects can be understood by constructing an accurate vibronic model for the absorption spectrum and have recently been described in detail for dye molecules in solution [46,47]. Of more interest for the present discussion is the finding that the decay timescale of

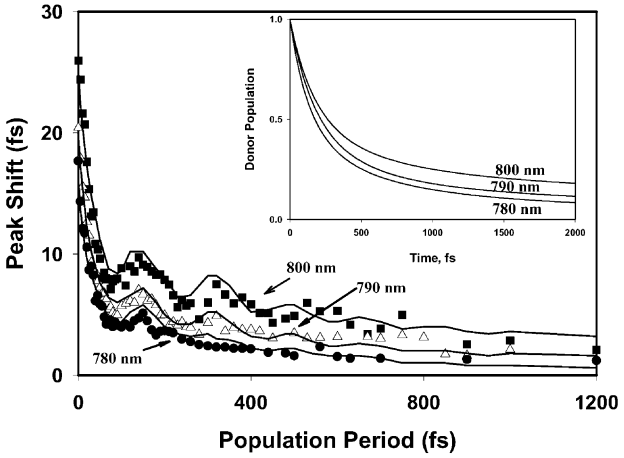

Fig. 7. Calculated peak shifts at 800, 790, and 780 nm based on the inhomogeneous hopping model described in the text. Inset shows the population kinetics for the three different excitation wavelengths. For clarity, the B800 to B850 energy transfer is not included in this plot, it is, however, properly included in the calculated peak shifts of the main figure.

the slower component in the peak shift (representing B800 to B800 energy transfer) decreases from about 600 fs at 800 nm to 500 fs at 790 nm and 400 fs at 780 nm.

Such an effect is characteristic of energy transfer in an inhomogeneous energy transfer system, because the pigments in the low energy position of the distribution have a much higher likelihood of making an 'uphill' energy transfer step. Fig. 7 shows the result of such calculations using a value of the inhomogeneous width $\Delta_{\mathrm{loc}} = 100\,\mathrm{cm}^{-1}$. Clearly, the experimental data are reproduced extremely well. The inset shows the decay of an initially populated donor at three different wavelengths. The wavelength dependent kinetics is obtained by filtering the Monte Carlo procedure by the laser spectrum. The more rapid decay at the higher energy side of the distribution is apparent. For clarity, the B800 to B850 transfer process is not included in the calculations shown in the inset, it is, however, properly included in the simulations of the experimental data.

To sum up, the energy transfer within the B800 ring of LH2 can be well understood as incoherent hopping on a timescale of ~500 fs via the Förster mechanism in an inhomogeneous ensemble. The inhomogeneity does not appear to have any correlation in individual aggregates beyond that expected from the limited sampling of the full distribution by the individual groups of B800 molecules. In other words, the energy transfer dynamics are dominated by the local disorder and the spatial correlation length of the factors responsible for the site energy variation is, therefore, not much larger than the spacing between molecules.

4. Nonlinear response of excitonically coupled systems

In the case of the B850 molecules of LH2 or the B875 molecules of LH1, the situation is more complicated and more interesting. Now the excitonic interactions are at least similar to the site energy disorder and to $k_{\mathrm{B}}T$ and the electronic states will be at least partially delocalized. This delocalization leads to the phenomenon of exchange narrowing [61–63], whereby the distribution of site energies is apparently narrowed by the averaging effect of the delocalized electronic states. Thus, the intra-complex disorder (and, therefore, the total disorder) associated with the delocalized states become dependent on J, the electronic coupling. The inter-complex disorder Σ, however, remains independent of J.

The third-order response function governing the nonlinear signals is described by a density matrix in the representation of the static-energy-dependent exciton basis which is, as usual, obtained by numerical diagonalization of Hamiltonian [64,65]. Zhang et al. formulated a third-order response function in this context based on the projection operator technique and applied it to photon echo and pump-probe studies of the B850 systems of LH2 [65]. The evolution equations for those density matrix elements are given by

$$\frac{\mathrm{d}}{\mathrm{d}t}\rho(t) = -i(L_0 + L')\rho(t) \tag{11}$$

where L_0 is a diagonal Liouville operator governing exciton dynamics in the absence of any exciton transfer process. The off-diagonal term, L', in Eq. (11) is responsible for the population transfer process between the exciton states and we employ a course-grained description for those population transfer processes

$$\frac{\mathrm{d}}{\mathrm{d}t}\rho(t) \approx iL_0\rho(t) - R\rho(t) \tag{12}$$

where the matrix R is given by the Redfield tensor which is based on a second-order approximation with respect to the off-diagonal coupling. Solution of Eq. (12) is combined with the expression for the polarization to give the third-order signal arriving from a given configuration of the static nuclear component. Finally, we use a take Monte Carlo sampling procedure in order to get the macroscopic polarization averaged over the random configuration of the static energies.

4.1. Application to LH1

The most crucial parameters determining the mechanism of the excitation energy transfer within LH1 are the Coulombic interaction and dynamic and static disorder of transition energies. Two-dimensional (2D) electron diffraction of LH1 reveals a larger ring very similar to B850 with 32 BChl, possibly segregated into pairs [10]. However, the resolution of this study is not sufficient to specify precisely microscopic parameters, such as the distances between pigments and the orientation of the transition dipole moments. Despite the importance of the LH1 complexes in the sequence of energy transfer from the LH2 to the reaction center, less extensive efforts have been made on the study of the LH1 complexes because of the lack of structural information.

Recently, Hu and Schulten suggested a model for the structure of LH1 of *Rb. sphaeroids* as a hexadecamer of αβ-heterodimers [66]. The characteristic structure of the basic unit of the complex is the same as in the B850 band of the LH2 complex. The model structure shows that the LH1 complex contains a ring of 32 BChls (18 BChls in the B850 band of the LH2) referred to as B875 BChls according to their main absorption band. The Mg–Mg distance between neighboring B875 BChls is 9.2 Å within the αβ-heterodimer and 9.3 Å between neighboring αβ-heterodimers which are surprisingly similar to those in the LH2 complex. Since the number of heterodimers in the LH1 and LH2 complexes differ by a factor of 2, the overall size and angle between the monomeric BChls must be different. Even though this difference could yield different values of the Coulombic coupling between the BChls in the LH1 compared to those of LH2, the similar intermolecular distances in the two complexes leads us to assume that the Coulombic coupling strength should be in the same order of magnitude. We will assume the circular structure suggested by Hu and Schulten and construct model Hamiltonians for LH1 and, for the purpose of comparison, the B850 band of LH2 and calculate the peak shift and absorption spectrum of the two complexes.

From the well-resolved structural information, the Coulombic coupling strengths in the LH2 complexes have been studied experimentally [67–72] and theoretically [59,60,73–78] to give a range of 200–800 cm^{-1}. With those relatively well established values of the Coulombic coupling, various experimental techniques have been used to determine the dynamic and static disorder [26,31,33]. Among those, we will take the parameter values which have been employed by Scholes and Fleming [79]. They determined the intra- and inter-dimer nearest neighbor Coulombic coupling strength as 320 and 255 cm^{-1}, respectively. The monomeric transition energies of two different types of BChl molecules within a dimer were suggested to be different by 530 cm^{-1}. By introducing a line broadening function (obtained by an analysis of 3PEPS data [31] with a simple two-level model), they obtained absorption and CD spectra in excellent accord with the experimental data. Since the CD spectrum is very sensitive to the variation of the parameters mentioned above [80], we assume the values they determined are quite reliable.

Fig. 8a shows the experimental peak shift behavior of the LH2 of *Rb. sphaeroids* at room temperature measured by Jimenez et al. [31]. The pulse width and center wavelength are 35 fs and 850 nm, respectively. By use of our model described in Section 4, we simulated the experimental data in Fig. 8a. Although one can see minor oscillatory features in the peak shift data which presumably arise from coherent vibrational motion, we ignore this effect in the present paper. The effect of nuclear motion is described only by one Gaussian component in the transition frequency correlation function, $M(t)$, which represents fast fluctuations of the chromophore and protein molecules: $M(t) = e^{-(t/\tau_g)^2}$ with $\tau_g =$ 150 fs. The reorganization energy for BChl-*a* monomer in the light harvesting complex is assumed to be 120 cm^{-1}. The effect of local static disorder is incorporated by a Gaussian distribution of transition energies of monomers ($\Delta_{loc} =$ 150 cm^{-1}) and the global static disorder is assumed not to exist ($\Sigma_{glob} = 0$). The current model calculation fits the peak shift rather well. With this set of parameters, the average of delocalization length (defined by the inverse participation ratio [57,81–83]) weighted by oscillator strength is obtained as 4.

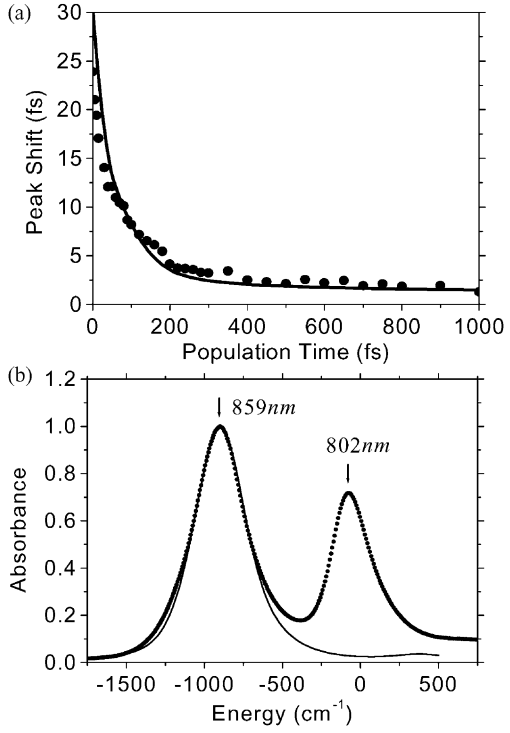

Fig. 8. Peak shift data (a) and absorption spectrum (b) of LH2 from *Rb. sphaeroids* (solid dots). The experimental data are from [31], the solid lines calculated using the theory outlined in the text.

With the same parameter set, we simulated the absorption spectrum as shown in Fig. 8b. Exchange narrowing and lifetime broadening of the line shape (resulting from dephasing process due to population transfer) as well as pure dephasing process are properly incorporated within the present model. The simulated absorption spectrum almost completely agrees with the experimental data with a minor deviation on the red side of the B850 band. The disagreement on the blue side around −500 cm^{-1} mainly results from our neglect of high frequency modes in the simulation in order to save calculation time. Also, the blue side of the absorption spectrum should have a small contribution from the B800 band, which is not taken into account in our simulation. From the comparison of simulations and experiments of the peak shift and absorption spectrum, we believe that spectral information associated with the BChl molecules in the B850 band of the LH2 complex are reasonably well quantified and will be described in detail elsewhere [84].

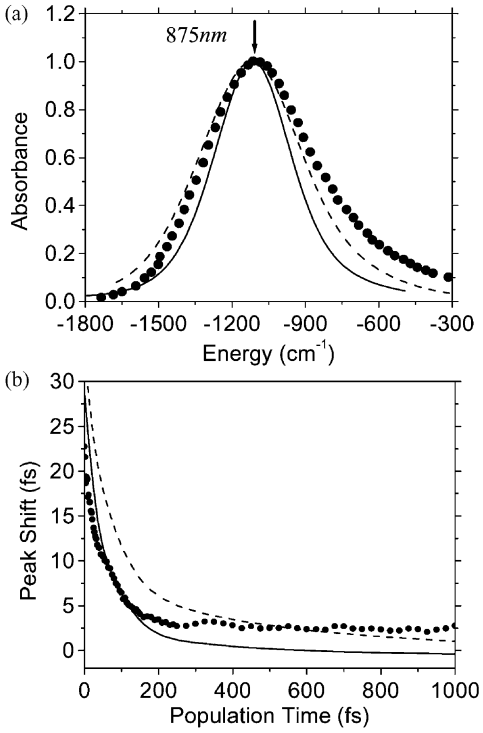

Fig. 9. Absorption spectrum (a) and peak shift data (b) for LH1 from *Rb. sphaeroids* (solid dots). The data are from [31], the solid lines from calculations using the LH2 parameter, the dashed line uses an inhomogeneous width (Δ_{loc}) of 250 cm^{-1} rather than 150 cm^{-1}.

Now we extend our calculations to the LH1 complex. For our initial calculations we employ the same values of parameters as used for LH2. In this case, the only difference between LH1 and LH2 is in the number of monomers included in each complex. Fig. 9a and b show the resulting peak shift and absorption spectrum, respectively, along with the experimental data measured by Jimenez et al. [31]. Neither experiment could be well reproduced with the LH2 parameter set.

The major differences between the simulation and the experiment lie in the long time value of the peak shift and line width of the absorption spectrum. The simulated peak shift for LH1 at long time is smaller than that for LH2. There are two possible origins for this effect and to obtain a physical picture, we base our discussion on previous results for an isolated two-level system. The delocalization scale of the exciton states in LH complexes is greater than one monomer and, thus, the contribution of transitions from one-exciton to two-exciton states will yield a somewhat different picture of the peak shift from that of an isolated two-level system. However, we believe such an approach will allow us to qualitatively understand the peak shift behavior of the exciton systems without relying on a complicated calculation. For a two-level system with moderate static disorder, Cho et al. [28] derived the long time value, $\tau^*(\infty)$, of the peak shift as:

$$\tau^*(\infty) \sim \frac{\Delta^2}{\Delta^3_{\mathrm{el-ph}}} \tag{13}$$

where Δ and $\Delta_{\mathrm{el-ph}}$ are the static disorder of the monomer and the electron–phonon coupling strength, respectively. Assuming the delocalized exciton states to be effective two-level systems, one could, in the absence of any exciton transfer process, approximately extend the applicability of Eq. (13) to the exciton system

$$\tau^*(\infty) \sim \frac{\Delta^2_{\mathrm{ex,in}}}{\Delta^3_{\mathrm{ex-ph}}} \tag{14}$$

where $\Delta_{\mathrm{ex,in}}$ and $\Delta_{\mathrm{ex-ph}}$ are the static disorder associated with the effective two-level exciton system and its coupling strength to the phonon. If the size of delocalization length is smaller than the size of whole aggregate, the former is approximated by

$$\Delta^2_{\mathrm{ex,in}} \approx \Sigma^2 + \frac{\sigma^2}{N_{\mathrm{del}}} \tag{15}$$

where Σ and σ are introduced in Section 2. Here N_{del} is the delocalization length of the exciton state. The first term in Eq. (15) describes the fluctuations of the mean energy of the aggregate and the second term is the exchange-narrowed intra-aggregate disorder of the exciton state. The exciton–phonon coupling strength is also exchange-narrowed and thus, if we neglect any exciton transfer process, we get $\Delta_{\mathrm{ex-ph}} = \Delta_{\mathrm{el-ph}}/\sqrt{N_{\mathrm{del}}}$ and the long-time peak shift is given by

$$\tau^*(\infty) \sim \frac{\Sigma^2 + \sigma^2/N_{\mathrm{del}}}{\Delta^3_{\mathrm{el-ph}}/N^{3/2}_{\mathrm{del}}} \tag{16}$$

This is an approximate expression for long time value of peak shift of the exciton system with a delocalization length N_{del} in the absence of any exciton transfer process. The exciton transfer can be approximately incorporated into Eq. (16) by using our previous studies on the peak shift of energy transfer systems [40,45]. Using these results, we infer that the peak shift in the presence of exciton transfer is given by

$$\tau^*(\infty) \sim \frac{\Sigma^2 + (\sigma^2/N_{\mathrm{del}})f_{\mathrm{i}}}{\Delta^3_{\mathrm{el-ph}}/N^{3/2}_{\mathrm{del}}} \tag{17}$$

where f_{i} is the fraction of the exciton population remaining on the initial states out of the total population of optically active exciton states. Physically the factor f_{i} describes how many optically active exciton states have a rephasing capability (associated with the intra-aggregate disorder) to give a finite peak shift. If the excitons stay in their initial states forever, $f_{\mathrm{i}} = 1$ and if all the excitons have moved to different states, $f_{\mathrm{i}} = 0$. In Eq. (17), we did not include a change in the effective exciton–phonon coupling strength due to lifetime broadening based on the assumption that the latter is smaller than the former. Inserting Eqs. (3), (5) and (6) into

Eq. (17), we finally get

$$\tau^*(\infty) \sim \frac{N_{\mathrm{del}}^{3/2}}{\Delta_{\mathrm{el-ph}}^3}\Sigma_{\mathrm{glob}}^2 + \sqrt{N_{\mathrm{del}}}\frac{\Delta_{\mathrm{loc}}^2}{\Delta_{\mathrm{el-ph}}^3}\left[\frac{N_{\mathrm{del}}}{N} + \frac{N-1}{N}f_{\mathrm{i}}\right]$$

$$\sim \frac{N_{\mathrm{del}}^{3/2}}{\Delta_{\mathrm{el-ph}}^3}\Sigma_{\mathrm{glob}}^2 + \sqrt{N_{\mathrm{del}}}\frac{\Delta_{\mathrm{loc}}^2}{\Delta_{\mathrm{el-ph}}^3}\left[\frac{N_{\mathrm{del}}}{N} + f_{\mathrm{i}}\right]$$

$$\text{when } N \gg 1 \tag{18}$$

The accuracy of this expression needs to be checked by comparison with the exact calculation discussed in Section 4 in future work. Looking at Eq. (18), we can see why the simulated 3PEPS data in the LH1 and LH2 have different offsets. Since we have used the same set of parameters, the delocalization length should be very similar in the calculations for the two complexes. Then only the differences come from Σ_{glob}, the number of monomers N and the factor f_{i} in Eq. (18). The N^{-1}-dependence on the second term comes from the effect of inter-aggregate fluctuation with a width Σ_{loc}. As N increases (LH1), the value of Σ_{loc} become reduced as shown by Eq. (5) to lower the rephasing capability associated with it. The factor f_{i} will also be inversely proportional to the value of N. As the number of monomers becomes larger, the number of excitons which have optical activity will also increase unless the exciton size change. Thus, the fraction of excitons staying on the initial state out of the full set of optically active states will be reduced as the number of monomers increases. As a result, we will get a reduced peak shift at long times. These mechanisms will not affect the absorption spectrum significantly (as shown in the simulation) since the total magnitude of disorder is not different. Since both mechanisms arise only from the difference in the number of monomers, they are related to each other.

Now, based on the intuition obtained from Eq. (18), we will try to fit the experimental data using exact simulations. From our studies on isolated two-level systems and Eq. (18), we know that the long time value of the peak shift can be increased by increasing the magnitude of the static disorder. Of course, this also makes the bandwidth of the absorption spectrum wider. Thus, in order to improve the agreement of simulation and the experimental data, one could try to employ a larger value of static disorder. The dashed lines in Fig. 9 represent the case of $\Delta_{\mathrm{loc}} = 250\,\mathrm{cm}^{-1}$. As expected, the bandwidth of the absorption spectrum is increased and the overall peak shift is moved up. However, we can clearly see that a slowly decaying component in the simulated peak shift data became more apparent. This decay results from energy hopping between exciton units (delocalized over a few monomers). As we increase the static disorder, exciton states become more localized and the energy gap between adjacent exciton states becomes larger. As a result, we see energy hopping process occurring on a longer time scale. In contrast to the simulated data, the experimental data show almost no decrease in the peak shift after about 400 fs. This means equilibration of the excitation within a circular ring is almost complete on this timescale. Increase of electron–phonon coupling strength will make the rate of exciton equilibration faster but also bring down the overall peak shift, which does not improve the fit of the simulated data to the experimental data. Since the bandwidth of the simulated absorption spectrum for $\Delta_{\mathrm{loc}} = 250\,\mathrm{cm}^{-1}$ is already broad enough, it would make no sense to increase the static disorder and electron–phonon coupling strength any more. The second possibility suggested by Eq. (18) to increase the long time value of peak shift is to reduce the electron–phonon coupling strength. However, this will significantly increase the initial peak shift and give a much larger disagreement with the experimental initial peak shift.

One solution to this problem is to introduce a non-zero value of Σ_{glob}. Since we perform a Monte Carlo simulation based on a Gaussian distribution of monomer energies, the inter-aggregate disorder originating from the statistical fluctuation is automatically incorporated in our previous simulation. Therefore, extra degrees of inter-aggregate disorder resulting from physical heterogeneity may be necessary in order to get a reasonable fit. In Fig. 10, we present the absorption spectrum and the 3PEPS simulated with the same parameters as in Fig. 9 except for introducing a Σ_{glob} of $50\,\mathrm{cm}^{-1}$ and the two vibrational modes previously captured in [31]. Even though a little fine-tuning in the simulated

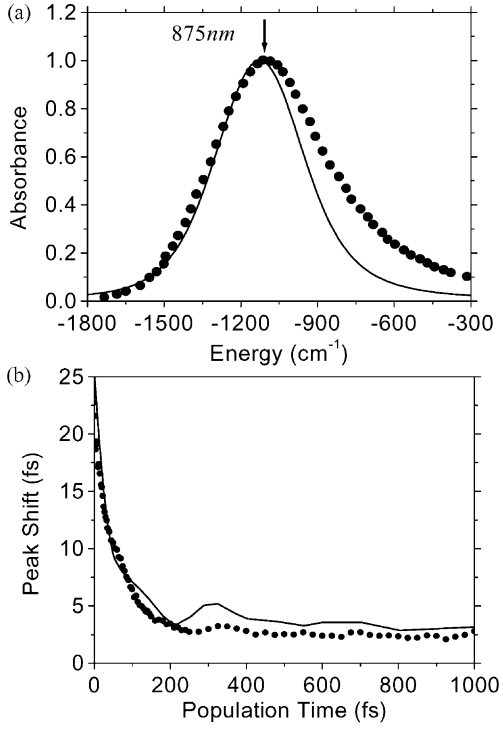

Fig. 10. Calculated absorption spectrum (a) and peak shift (b) for LH1 (lines) compared with experimental data (solid dots) for a model including global heterogeneity between complexes ($\Sigma_{\mathrm{glob}} = 50\,\mathrm{cm}^{-1}$). The two vibrational modes (with the frequencies 110 and $190\,\mathrm{cm}^{-1}$) captured in [31] are included. The other parameters remain the same as in Fig. 9.

3PEPS is required, we could get much improved fits of both the absorption and the 3PEPS data.

Another insight from Eq. (18) is that the long time value of the peak shift is proportional to the delocalization length. Thus, in order to increase the simulated peak shift in Fig. 9, we could try to increase the delocalization length. Increase of the electronic coupling strength only, will make the absorption spectrum too narrow due to strong exchange narrowing. Instead, therefore, we increase the static disorder, Δ_{loc}, as well as the electronic coupling strength. Fig. 11 shows a simulation with three parameter sets that give $N_{\mathrm{del}} = 8$ ($\Delta_{\mathrm{loc}} = 105\,\mathrm{cm}^{-1}$, $J = 400\,\mathrm{cm}^{-1}$), ($\Delta_{\mathrm{loc}} = 185\,\mathrm{cm}^{-1}$, $J = 600\,\mathrm{cm}^{-1}$), ($\Delta_{\mathrm{loc}} = 225\,\mathrm{cm}^{-1}$, $J = 700\,\mathrm{cm}^{-1}$), while the reorganization energy and Σ_{glob} are fixed to $240\,\mathrm{cm}^{-1}$ and 0, respectively. The last set of parameters gives the best fit to the experimental data.

If we accept the increased coupling model, the calculations shown in Fig. 11 suggest that the excitonic states are somewhat more delocalized in LH1 than those of LH2. The superradiance studies of Monshouwer et al. [83] find emitting dipole strengths (relative to bacteriochlorophyll *a*) of 2.8 for LH2 and 3.8 for LH1. To avoid confusion, we note that the dipole strengths refer to the equilibrated (long time) state, whereas our N_{del} refers to the initially prepared exciton states. The two pairs of number cannot be compared directly, but their ratios are similar for LH1:LH2, and we would clearly expect the delocalization to be less in the equilibrium state, thus, the two measures are consistent. However, to definitively decide between the two possible interpretations of our LH1 data: increased coupling, increased Δ_{loc} versus introduction of Σ_{glob} requires more modeling-for example of the CD spectrum.

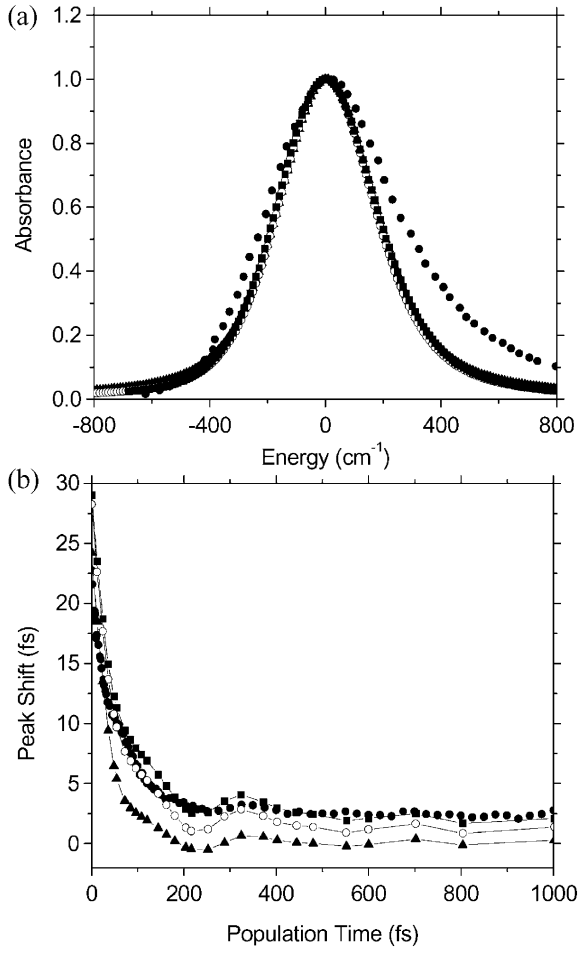

Fig. 11. Effect of increasing the electronic coupling (J) and the disorder (Δ_{loc}) on the calculated LH1 absorption spectrum (a) and peak shift (b). Again the experimental data are shown with solid dots. $\Delta_{\mathrm{loc}} = 105\,\mathrm{cm}^{-1}$, $J = 400\,\mathrm{cm}^{-1}$ (solid triangle), $\Delta_{\mathrm{loc}} = 185\,\mathrm{cm}^{-1}$, $J = 600\,\mathrm{cm}^{-1}$ (open circle), $\Delta_{\mathrm{loc}} = 225\,\mathrm{cm}^{-1}$, $J = 700\,\mathrm{cm}^{-1}$ (solid square). Σ_{glob} is fixed at zero and the reorganization energy is $240\,\mathrm{cm}^{-1}$ in all cases.

In either case, the dynamical behavior in both LH1 and LH2 (B850) is clearly rather different from that in B800 of LH2. In our model, the relaxation process occurring on the 100 fs timescale corresponds to relaxation between partially delocalized exciton states, with a timescale controlled by the exciton–phonon coupling strength. However, investigation of the wavefunctions of the exciton states of individual complexes, in the context of the model outlined in Section 4, suggests a relatively simple picture for the spatial motion of the excitation. The relaxation within the exciton manifold of a given complex is controlled by the energy gap between the exciton states and the spatial overlap of their wavefunctions. On the average, using the parameters of Figs. 8 and 11, the individual exciton states are initially delocalized over four and eight monomers in LH2 and LH1, respectively. The overlap requirement then implies a picture of the excitation moving between groups of monomers, since to a good approximation in LH2, and a reasonable approximation in LH1, the non-zero amplitudes of the wavefunctions are concentrated on neighboring molecules. In other words, a reasonable crude picture of the spatial motion of excitation in LH2 (B850) and LH1 (as a result of exciton relaxation) is of hopping between groups of molecules, rather than hopping between monomers as in B800 of LH2.

5. Concluding remarks

The light harvesting antenna of purple bacteria is based on an energy funnel beginning with B800 and proceeding via B850 and B875 to the reaction center. There are two obvious ways to construct such a funnel: (1) select different chemical species that absorb at the required wavelengths or (2) use exciton (and solvation) interactions to progressively red shift the spectra of the same chemical species. In the purple bacteria, nature has adopted the second strategy and it is tempting to speculate on whether there is an intrinsic advantage to this solution (ignoring completely any biosynthetic implications of the first solution). To effectively and efficiently transfer energy between many identical molecules, it is important to avoid losing too much energy per step. This, in turn, implies that both homogeneous and inhomogeneous contributions to the lineshape should be relatively small. In

the excitonic system, the phenomenon of exchange narrowing reduces the intrinsic values of both broadening contributions. Relatively weak electron–phonon coupling can induce rapid spatial motion of the exciton, without a large loss in energy (and consequent decrease in Franck–Condon factor) because of the exchange narrowing. Similarly, the influence of static variations of site energies, which are presumably inevitable in natural systems, is substantially decreased by the exchange narrowing. Both effects are somewhat reduced by the lifetime broadening effect of the exciton relaxation, but overall there is a significant reduction in linewidth in both B850 and B875. In contrast, in B800, up to a reasonable level, disorder is not a major problem since the transfer to B850 is significantly downhill.

With our present knowledge, it is not possible to say definitively whether the delocalization is simply a consequence of the excitonic red shift or an important design feature. Such questions are likely to provoke spectroscopic studies of antenna systems for many years to come.

Acknowledgements

G.R.F. thanks Lord Porter for support and encouragement over the past 30 years, and for inspiring our studies of photosynthetic energy transfer. This work was supported by the Director, Office of Science, Office of Basic Energy Sciences, Chemical Sciences Division, of the US Department of Energy under Contract no. DE-AC03-76SF0098.

References

[1] G.S. Beddard, G. Porter, C.J. Tredwell, Nature 258 (1975) 166.
[2] M. Seibert, R.R. Alfano, S.L. Shapiro, Biochim. Biophys. Acta 292 (1973) 493.
[3] M. Seibert, R.R. Alfano, Biophys. J. 14 (1974) 269.
[4] S.L. Shapiro, V.H. Kollman, A.J. Campillo, FEBS Lett. 54 (1975) 358.
[5] G. Porter, C.J. Tredwell, G.F.W. Searle, J. Barber, Biochim. Biophys. Acta 501 (1978) 232.
[6] G.S. Beddard, G. Porter, Nature 260 (1976) 366.
[7] G. McDermott, S.M. Prince, A.A. Freer, A.M. Hawthornthwaite-Lawless, M.Z. Papiz, R.J. Codgell, N.W. Isaacs, Nature 374 (1995) 517.
[8] A.A. Freer, S. Prince, K. Sauer, M.Z. Papiz, A.M. Hawthornthwaite-Lawless, G. McDermott, R.J. Cogdell, N.W. Isaacs, Structure 4 (1996) 449.
[9] J. Koepke, X. Hu, C. Muenke, K. Schulten, H. Michel, Structure 4 (1996) 581.
[10] S. Karrasch, P.A. Bullough, R. Ghosh, EMBO J. 14 (1995) 631.
[11] D.E. Tronrud, M.F. Schmidt, B.E. Matthews, J. Mol. Biol. 188 (1986) 443.
[12] Y.F. Li, W. Zhou, R.E. Blankenship, J.P. Allen, J. Mol. Biol. 271 (1997) 456.
[13] N. Krauss, W.-D. Schubert, O. Klukas, P. Fromme, H.T. Witt, W. Saenger, Nature Struct. Biol. 3 (1996) 965.
[14] J. Deisenhofer, O. Epp, K. Miki, R. Huber, H. Michel, Nature 318 (1985) 618.
[15] H. Michel, O. Epp, J. Deisenhofer, EMBO J. 5 (1986) 2445.
[16] J.P. Allen, G. Feher, T.O. Yeates, H. Komiya, D.C. Rees, Proc. Natl. Acad. Sci. U.S.A. 84 (1987) 5730.
[17] J.P. Allen, G. Feher, T.O. Yeates, H. Komiya, D.C. Rees, Proc. Natl. Acad. Sci. U.S.A. 84 (1987) 6162.
[18] A. Adronov, S.L. Gilat, J.M.J. Fréchet, K. Ohta, F.V.R. Neuwahl, G.R. Fleming, J. Am. Chem. Soc. 122 (2000) 1175.
[19] H.A. Frank, R.J. Cogdell, in: A. Young, G. Britton (Eds.), Carotenoids in Photosynthesis, Chapman & Hall, London, 1993, p. 252.
[20] H. Nagae, T. Kakitani, T. Katoh, M. Mimuro, J. Chem. Phys. 98 (1993) 8012.
[21] A. Damjanovic, T. Ritz, K. Schulten, Phys. Rev. E 59 (1999) 3293.
[22] J.-P. Zhang, R. Fujii, P. Qian, T. Inaba, T. Mizoguchi, Y. Koyama, K. Onaka, Y. Watanabe, H. Nagae, J. Phys. Chem. B 104 (2000) 3683.
[23] D.L. Dexter, J. Chem. Phys. 21 (1953) 836.
[24] P.J. Walla, P.A. Linden, C.-P. Hsu, G.D. Scholes, G.R. Fleming, Proc. Natl. Acad. Sci. U.S.A. 97 (2000) 10808.
[25] C.-P. Hsu, P.J. Walla, G.R. Fleming, M. Head-Gordon, J. Phys. Chem. B, in press.
[26] T. Joo, Y.W. Jia, J.-Y. Yu, D.M. Jonas, G.R. Fleming, J. Phys. Chem. 100 (1996) 2399.
[27] T. Joo, Y.W. Jia, J.-Y. Yu, M.J. Lang, G.R. Fleming, J. Chem. Phys. 104 (1996) 6089.
[28] M. Cho, J.-Y. Yu, T. Joo, Y. Nagasawa, S.A. Passino, G.R. Fleming, J. Phys. Chem. 100 (1996) 11944.
[29] S.A. Passino, Y. Nagasawa, T. Joo, G.R. Fleming, J. Phys. Chem. A 101 (1997) 725.
[30] Y. Nagasawa, S.A. Passino, T. Joo, G.R. Fleming, J. Chem. Phys. 106 (1997) 4840.
[31] R. Jimenez, F. van Mourik, J.-Y. Yu, G.R. Fleming, J. Phys. Chem. B 101 (1997) 7350.
[32] S.A. Passino, Y. Nagasawa, G.R. Fleming, J. Chem. Phys. 107 (1997) 6094.
[33] J.-Y. Yu, Y. Nagasawa, R. van Grondelle, G.R. Fleming, Chem. Phys. Lett. 280 (1997) 404.
[34] Y. Nagasawa, J.-Y. Yu, M. Cho, G.R. Fleming, Faraday Discussions 108 (1997) 23.
[35] M.L. Groot, J.-Y. Yu, R. Agarwal, J.R. Norris, G.R. Fleming, J. Phys. Chem. B 102 (1998) 5923.
[36] Y. Nagasawa, Y.-Y. Yu, G.R. Fleming, J. Chem. Phys. 109 (1998) 6175.
[37] M. Yang, G.R. Fleming, J. Chem. Phys. 110 (1999) 2983.
[38] M.J. Lang, X.J. Jordanides, X. Song, G.R. Fleming, J. Chem. Phys. 110 (1999) 5884.
[39] M. Yang, K. Ohta, G.R. Fleming, J. Chem. Phys. 110 (1999) 10243.
[40] M. Yang, G.R. Fleming, J. Chem. Phys. 111 (1999) 27.
[41] X.J. Jordanides, M.J. Lang, X. Song, G.R. Fleming, J. Phys. Chem. B 103 (1999) 7995.
[42] D.S. Larsen, K. Ohta, G.R. Fleming, J. Chem. Phys. 111 (1999) 8970.
[43] Q.-H. Xu, G.D. Scholes, M. Yang, G.R. Fleming, J. Phys. Chem. A 103 (1999) 10348.
[44] R. Agarwal, B.P. Krueger, G.D. Scholes, M. Yang, J. Yom, L. Mets, G.R. Fleming, J. Phys. Chem. B 104 (2000) 2908.
[45] M. Yang, G.R. Fleming, J. Chem. Phys. 113 (2000) 2823.
[46] D.S. Larsen, K. Ohta, Q.-H. Xu, G.R. Fleming, J. Chem. Phys., submitted for publication.
[47] K. Ohta, D.S. Larsen, M. Yang, G.R. Fleming, J. Chem. Phys., submitted for publication.
[48] W.P. de Boeij, M.S. Pshenichnikov, D.A. Wiersma, J. Phys. Chem. 100 (1996) 11806.
[49] W.P. de Boeij, M.S. Pshenichnikov, D.A. Wiersma, Ann. Rev. Phys. Chem. 49 (1998) 99.
[50] R. Agarwal, M. Yang, Q.-H. Xu, G.R. Fleming, J. Phys. Chem. B 105 (2001) 1887.
[51] E. Gudowska-Nowak, M.D. Newton, J. Fajer, J. Phys. Chem. 94 (1990) 5795.
[52] A. Freiberg, K. Timpmann, R. Ruus, N.W. Woodbury, J. Phys. Chem. B 103 (1999) 10032.

[53] A.M. van Oijen, M. Ketelaars, J. Köller, T.J. Aartsma, J. Schmidt, Biophys. J. 78 (2000) 1570.
[54] M.V. Mostovoy, J. Knoester, J. Phys. Chem. B 104 (2000) 12355.
[55] S.E. Dempster, S. Jang, R. Silbey, J. Chem. Phys., submitted for publication.
[56] J.M. Jean, C.-K. Chan, G.R. Fleming, Israel J. Chem. 28 (1988) 169.
[57] V. Sundström, T. Pullerits, R. van Grondelle, J. Phys. Chem. B 103 (1999) 2327.
[58] Y.-Z. Ma, R.J. Cogdell, T. Gillbro, J. Phys. Chem. B 102 (1998) 881.
[59] B.P. Krueger, G.D. Scholes, G.R. Fleming, J. Phys. Chem. B 102 (1998) 5378.
[60] G.D. Scholes, I.R. Gould, R.J. Cogdell, G.R. Fleming, J. Phys. Chem. B 103 (1999) 2543.
[61] E.W. Knapp, Chem. Phys. 85 (1984) 73.
[62] J. Knoester, J. Chem. Phys. 99 (1993) 8466.
[63] M. Wubs, J. Knoester, Chem. Phys. Lett. 284 (1998) 63.
[64] T. Meier, V. Chernyak, S. Mukamel, J. Chem. Phys. 107 (1997) 8759.
[65] W.M. Zhang, T. Meier, V. Chernyak, S. Mukamel, J. Chem. Phys. 108 (1998) 7763.
[66] X. Hu, K. Schulten, Biophys. J. 75 (1998) 683.
[67] T. Pullerits, V. Sundström, Acc. Chem. Res. 29 (1996) 381.
[68] T. Pullerits, M. Chachisvilis, V. Sundström, J. Phys. Chem. 100 (1996) 10787.
[69] R. van Grondelle, J.P. Dekker, T. Gillbro, V. Sundström, Biochim. Biophys. Acta 1187 (1994) 1.
[70] A. Freiberg, J.A. Jackson, S. Lin, N.W. Woodbury, J. Phys. Chem. A 102 (1998) 4372.
[71] M.H.C. Koolhaas, G. van der Zwan, R.N. Frese, R. van Grondelle, J. Phys. Chem. B 101 (1997) 7262.
[72] M.H.C. Koolhaas, G. van der Zwan, R. van Grondelle, J. Phys. Chem. B 104 (2000) 4489.
[73] K. Sauer, R.J. Cogdell, S.M. Prince, A. Freer, N.W. Issacs, H. Scheer, Photochem. Photobiol. 64 (1996) 564.
[74] X. Hu, T. Ritz, A. Demjanovic, K. Schulten, J. Phys. Chem. B 101 (1997) 3854.
[75] R.G. Alden, E. Johnson, V. Nagarajan, W.W. Parson, C.J. Law, R.G. Cogdell, J. Phys. Chem. B 101 (1997) 4667.
[76] J. Linnanto, J.E.I. Korppi-Tommola, V.M. Helenius, J. Phys. Chem. B 103 (1999) 8739.
[77] S. Tretiak, C. Middleton, V. Chernyak, S. Mukamel, J. Phys. Chem. B 104 (2000) 4519.
[78] S. Tretiak, C. Middleton, V. Chernyak, S. Mukamel, J. Phys. Chem. B 104 (2000) 9540.
[79] G. Scholes, G.R. Fleming, J. Phys. Chem. B 104 (2000) 1854.
[80] M.H.C. Koolhaas, G. van der Zwan, R.N. Frese, R. van Grondelle, J. Phys. Chem. B 101 (1997) 7262.
[81] H. Fidder, J. Knoester, D.A. Wiersma, J. Chem. Phys. 95 (1991) 7880.
[82] R. Jimenez, S.N. Dikshit, S.E. Bradforth, G.R. Fleming, J. Phys. Chem. 100 (1996) 6825.
[83] R. Monshouwer, M. Abrahamsson, F. van Mourik, R. van Grondelle, J. Phys. Chem. B 101 (1997) 7241.
[84] M. Yang, G.R. Fleming, in preparation.